What drove the Stony Coral Tissue Loss Disease outbreak in Florida

Thomas Dobbelaere [1,*], **Erinn Muller** [2], **Lewis Gramer** [3,4], **Dan Holstein** [5] and **Emmanuel Hanert** [1,6]

[1] Earth and Life Institute (ELI), UCLouvain, Louvain-la-Neuve, Belgium
[2] Coral Health and Disease Program, Mote Marine Laboratory, Sarasota, FL, USA
[3] Cooperative Institute for Marine and Atmospheric Studies (CIMAS), University of Miami, Miami, FL, USA
[4] Atlantic Oceanographic and Meteorological Laboratory (AOML), NOAA, Miami, FL, USA
[5] Department of Oceanography and Coastal Sciences, College of the Coast and Environment, Louisiana State University, Baton Rouge, LA, USA
[6] Institute of Mechanics, Materials and Civil Engineering (IMMC), UCLouvain, Louvain-la-Neuve, Belgium

Correspondence*:
Earth and Life Institute (ELI), UCLouvain, Croix du Sud 2 box L7.05.16, B-1348 Louvain-la-Neuve, Belgium
thomas.dobbelaere@uclouvain.be

ABSTRACT

For about six years, the Florida Reef Tract (FRT) has been experiencing an outbreak of the Stony Coral Tissue Loss Disease (SCTLD). First reported off the coast of Miami-Dade County in 2014, the SCTLD has since spread throughout the entire FRT with the exception of the Dry Tortugas. However, the causative agent for this outbreak is currently unknown. Here we show how a high-resolution bio-physical model with a modified patch SIR epidemic model can inform on the potential characteristics of the causative agent of the disease and its vector. In this study, the agent is assumed to be transported within composite material (such as coral mucus, dying tissues and/or resuspended sediments) driven by currents and potentially persisting in the water column for extended periods of time. In this framework, our simulations suggest that the SCTLD is likely to be propagated within neutrally buoyant materials driven by mean barotropic currents. Calibration of our model parameters with field data show that corals are then infected within a mean transmission time of 6.45 days. Furthermore, the propagation speed of the disease through the FRT is shown to be very sensitive to the value of an infection threshold, defined the proportion of infectious corals that causes an exponential growth of the disease on the colony. Our results present a new connectivity-based approach to understand the spread of the SCTLD through the FRT. Such method can provide a valuable complement to field observations and lab experiments to support the management of the epidemic as well as the identification of its causative agent.

Keywords: stony-coral-tissue-loss disease, biophysical modeling, Florida reef tract, spatial epidemiology, connectivity

1 INTRODUCTION

Coral diseases are a major threat to coral reef ecosystems and have led to significant declines in coral cover especially within the Caribbean region (Richardson et al., 1998; Sutherland et al., 2004; Aronson and

Precht, 2001; Harvell et al., 2007; Miller et al., 2009; Brandt and McManus, 2009). Indeed, the Florida reef tract, which was dominated by Acropora palmata and Acropora cervicornis, and often had 30% coral cover until the 1970s/80s (Dustan and Halas, 1987; Porter and Meier, 1992), is now dominated by bare substrate, octocorals, and macroalgae with only approximately 5% stony coral cover remaining (Ruzicka et al., 2013). The loss of the branching Acroporid species was attributed primarily to a disease outbreak, termed white band disease (Aronson and Precht, 2001), but several other threats such as habitat reduction, eutrophication, overfishing, and bleaching likely all contributed to these species decline (Team, 2005). Subsequent losses of coral cover within the region were often linked to additional disease incidences and repeated regional coral bleaching events as a result of global climate change (Kuta and Richardson, 1996; Richardson et al., 1998; Sutherland et al., 2004; Gardner et al., 2003; Aronson and Precht, 2006; Kuffner et al., 2015; Manzello, 2015). A novel coral disease outbreak, termed Stony Coral Tissue Loss Disease (SCTLD), is now threatening the last vestiges of coral throughout the Florida reef tract.

SCTLD was first documented off the coast of Miami-Dade County in the summer of 2014 by Precht et al. (2016) and has since spread throughout the entire Florida reef tract with the exception of the Dry Tortugas. To date, SCTLD has been observed affecting over 20 different stony corals species. A case definition of SCTLD has been compiled to describe the visual appearance and ecology of SCTLD (NOAA, 2018). Briefly, the gross morphology of SCTLD is described as focal or multifocal, with locally extensive to diffuse areas of acute to subacute tissue loss distributed basally, peripherally, or both. In some cases, tissues bordering areas of chronic tissue loss show indistinct bands (1–5 cm) of pallor, progressing to normal pigmentation away from the denuded skeleton. There is also a range in coral susceptibility to SCTLD, with species categorized as highly susceptible (e.g., Dendrogyra cylindrus, Dichocoenia stokesii, Meandrina meandrites), moderately susceptible (e.g., Orbicella spp., Montastraea cavernosa, Siderastrea siderea, Stephanocoenia intersepta), or tolerant (e.g., Porites spp., Acropora spp.). Unfortunately, SCTLD has not remained isolated in the Florida reef tract and has now been recorded in Mexico (Alvarez-Filip et al., 2019), the USVI (Blondeau et al., 2020) and several other location around the Caribbean. The continued persistence of the outbreak, the high number of species affected, and the large geographical range of reports consistent with the case definition suggests that SCTLD is the largest coral disease outbreak ever recorded.

Large-scale spatial epidemiologic analyses showed that the reefs in Florida with SCTLD are clustered, supporting a contagious mode of transmission (Muller et al., 2020). Similarly, aquaria-based experiments indicate SCTLD can be transmitted through direct contact or indirectly through the water column (Aeby et al., 2019) suggesting water can be a SCTLD vector, at least within a controlled setting. The initial exponential increase in spread among reefs from the disease epicenter (Precht et al., 2016) and the persistent subsequent linear rate of spread of SCTLD (Muller et al., 2020), north along South Florida reefs and south into the Florida Keys, indicates that water currents may play a role in disease transmission. Furthermore, the rate of spread, estimated at 100 m per day, suggests surface currents are likely too fast to have spread SCTLD within the region. These results imply that the bottom boundary layer, which is significantly slower than surface currents, may be the vertical layer in which transmission occurs (Aeby et al., 2019). However, to date, there have been no efforts linking local hydrodynamic modeling efforts with the spatio-temporal dynamics of SCTLD in Florida.

Estimating the transport of infectious material from reef to reef by currents cannot be performed empirically. However, experimentally-calibrated numerical models that simulate currents can provide a realistic picture of the dispersal of infected matters. Nonetheless, accurately modeling water circulation at the spatial scales that affect this dispersal remains a key challenge, as small-scale flow features such as recirculation eddies around reefs and islands strongly impact exchanges between reefs (Wolanski, 1994;

67 Burgess et al., 2007; Figueiredo et al., 2013). In this context, models that can explicitly simulate flow
68 features down to the reef scale are needed. This represents a spatial resolution of the order of 100-1,000 m
69 in dense reef systems. As of today, most regional ocean models using traditional numerical methods cannot
70 achieve such resolution because of the computational resources it requires. To our knowledge, the best
71 resolution currently available among these models in the FRT is $\sim$ 900 m with the FKEYS-HYCOM model
72 that has been developed for the Florida Keys region (Kourafalou and Kang, 2012; Sponaugle et al., 2012;
73 Vaz et al., 2016). Unstructured-mesh ocean models offer a potential solution to this resolution issue by
74 locally increasing the model resolution close to reefs and islands (Lambrechts et al., 2008; Thomas et al.,
75 2014, 2015), in order to focus the computational resources where they are most needed. High resolution
76 bio-physical dispersal models can be used to build the potential connectivity between reefs and therefore
77 approximate exchanges between colonies in the complex topography of the coral reef systems (Frys et al.,
78 2020).

79 Marine diseases differ significantly from better studied terrestrial diseases, namely due to the potential
80 for long environmental residence times, during which pathogens may survive and disperse through the
81 water (Harvell et al., 2007; Sokolow, 2009). Several recent studies have attempted to adapt traditional
82 epidemic models (Susceptible-Infectious-Recovered, or SIR models) to coral reef systems (Sokolow, 2009;
83 Bidegain et al., 2016a,b). Novel approaches have included developing pathogen pools (Bidegain et al.,
84 2016a,b), and to model at the metapopulation scale, rather than at the scale of coral holobionts (Sokolow,
85 2009). Both these approaches are attempting to address the same issue: Infection occurs between patches of
86 entirely sessile animals, through the dispersal of pathogen(s). Thus, there are internal within-patch disease
87 dynamics and metapopulation-scale between-patch dynamics occurring simultaneously. The epidemic
88 model developed in this study utilizes the same basic architecture of previous coral reef SIR models, but
89 rather than assume pathogen pools (e.g. Bidegain et al. (2016a,b)) or ignore internal patch dynamics (e.g.
90 Sokolow (2009)), we have modeled both within-patch disease dynamics and the dispersal of pathogen
91 explicitly using potential connectivity networks.

92 The objective of this study is to deduce the probable propagation mechanism of the SCTLD throughout
93 the FRT by developing an experimentally-calibrated epidemio-hydrodynamic model. With a resolution of
94 about 100 m, this model can capture potential exchanges of infectious matter between reefs that would
95 be ignored by coarser models. By reproducing the observed spread of disease between 1st May 2018 and
96 1st April 2014, we provide insight on the characteristics of the disease agent and its vector. Ultimately,
97 our model, coupled with lab and field works, would support the management of the epidemic and the
98 identification of its causative agent.

2 METHODS

2.1 Modeling reef connectivity

100 In this study, we focus on the exchanges of infectious material between coral reefs driven by ocean
101 currents, which therefore have to be accurately simulated. An ocean model should provide a realistic
102 large-scale circulation while also resolving small-scale flow features down to the scale of individual reefs.
103 In this study, we use the unstructured-mesh depth-integrated coastal ocean model SLIM[1] to simulate ocean
104 currents over an area that includes the FRT but also the Florida Strait and part of the Gulf of Mexico (Fig.
105 1). By using an unstructured mesh, we can increase the model resolution only over the FRT and hence
106 concentrate computational resources where they are most needed. SLIM , being a depth-averaged model, is

---

[1] https://www.slim-ocean.be
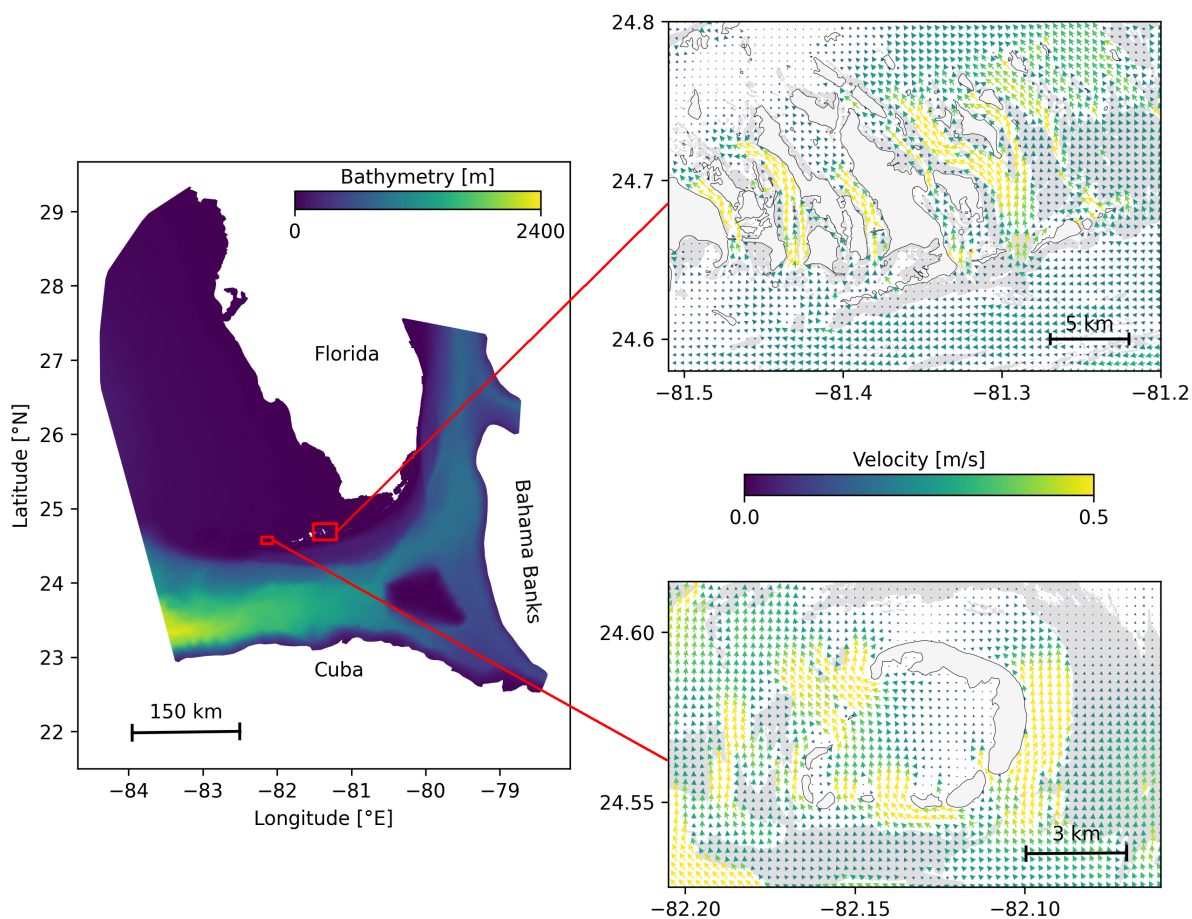
Figure 1. Model computational domain with the bathymetry (left) and close-up views of the mesh with snapshots of the currents on May, 25 2018 at 00:00, for the Marquesas Keys (bottom) and the Lower Keys (top). This illustrates the benefits of unstructured meshes to represent the fine-scale details of the topography and hence simulate currents down to the scale of individual reefs (shown in darker grey) and islands (shown in lighter grey with black contours).

107   well suited to shallow-water flows. Details of the model formulation and validation are provided in Frys
108   et al. (2020).

109   The mesh resolution depends only on the distance to the coast but we distinguish between the coastlines
110   along the FRT where we impose a maximum resolution of 100 m and the other coastlines along which
111   the maximum resolution is 2500 m. The mesh has been generated with the open-source mesh generator
112   GMSH (Geuzaine and Remacle, 2009) and has about 7×10^5 elements. The coarsest elements, far away
113   from the FRT, have a size of about 10 km. An illustration of ocean currents simulated on that mesh are
114   shown in Fig. 1. It shows how a 100-m spatial resolution allows us to simulate fine-scale details of the flow,
115   such as recirculation eddies and currents within the dense reef system in the Lower Keys that consist of
116   many individual reefs with narrow passages in between.

117   The simulated currents can then be used to model dispersal of infectious material throughout the FRT.
118   In this study, 3 types of potential vector carrying the disease causative agent were considered: positively
119   buoyant (e.g. mucus and surfactant), neutrally buoyant (e.g. fines, pelagic organisms) and negatively
120   buoyant (e.g. sediments, composites, demersal organisms). As SLIM is a depth-averaged model, the
121   mean currents it generates are well suited to model the dispersal of neutrally buoyant material remaining

122 within the water column. However, these currents must be modified to correctly represent the dynamics
123 of materials evolving in the surface and bottom boundary layers. Therefore, surface current response to
124 winds is estimated by adding 1.5% of the wind speed to SLIM currents with a windage angle of 45° to the
125 right for positively buoyant particles. Such parametrization is shown to be an accurate approximation of
126 wave-induced Stokes drift and quasi-Eulerian surface currents by (Ardhuin et al., 2009). For negatively
127 buoyant materials, on the other hand, bottom currents are obtained by taking 60% of SLIM currents
128 velocity with a veering angle of 15° to the left. **[Some references about the parametrization for bottom**
129 **currents]**

130   Using these three velocity fields, virtual particles are then released on all the reefs composing the FRT to
131 model the dispersal of infected materials carrying the disease causative agent. The locations of the reefs of
132 Florida are extracted from the "coral reefs and hardbottom" layer of the Unified Florida Reef Tract Map
133 (FWC, 2017). The polygon of this reef map are then further divided into 500 m squares in order to track the
134 propagation of the disease with a finer geographical resolution, generating a total of 16823 polygons. At
135 the beginning of each simulated months and for each type of currents, a total of about 1.5×10^6 particles
136 are released over all the reef polygons. These particles have a state composed of their polygon of origin
137 as well as their mass, initialized to 1, that they loose at a constant rate γ as they are moved by surface,
138 mean or bottom currents. In this study, the value of γ is chosen so that particles have a half life of 30
139 days. When the particles are brought over reef polygons by currents, the amount of infected mass that
140 lands on the polygon is recorded in monthly potential connectivity matrices whose entries are denoted
141 C_{ij}. The matrix rows correspond to the source reefs and the columns correspond to the destination reefs.
142 Hence C_{ij} represents the mass of infected material originating from sub-reef i that has settled on sub-reef j.
143 This matrix is then normalized by dividing each of its rows i by the the total mass of particles released on
144 polygon i in order to obtained the normalized potential connectivity matrix $\tilde{C}$, whose entry $\tilde{C}_{ij}$ gives the
145 probability that infectious material produced on sub-reef i settles on sub-reef j. Connectivity matrices are
146 computed for each type of current and for each month of the simulated period.

147   These connectivity matrices can be more easily handled by interpreting them as large graphs whose
148 vertices are reefs. They can then be analyzed using graph theory tools. In this study, four potential
149 connectivity measures are used to interpret the monthly computed graphs. These indicators are described
150 in Table 1. The first indicator is the weighted connectivity length (WCL), that gives the average dispersal
151 distance from origin to destination for material produced on a given reef. The weighted connectivity of reef
152 polygon i writes:

$$WCL_i = \frac{\sum_j \tilde{C}_{ij} L_{ij}}{\sum_j \tilde{C}_{ij}} \tag{1}$$

153 where L_{ij} is the distance between origin reef i and destination reef j. Another measure of the spreading
154 potential of reef j is its out-degree, *i.e.* the product of the number of connections originating from reef j
155 by the quantity of infectious matter its sends to the network. This indicator is obtained by computing the
156 number non-zero entries of row i of the potential connectivity matrix C and multiplying it with $\sum_j C_{ij}$. The
157 information given by the out-degree is complemented by the proportion of infectious elements produced
158 on reef i that successfully settles on a reef, called the fraction exchanged of reef i. This indicator is
159 given by $\sum_j \tilde{C}_{ij}$. Finally, the isolation of reef i in the network is given by the self recruitment, *i.e.* the
160 proportion of infectious matter settling on reef i that originates from reef i, computed by $C_{ii}/\sum_j C_{ji}$. A
161 large self-recruitment value indicates that few infectious matter produced elsewhere settles on the reef and
162 thus that it is isolated from the rest of the network.

Indicators	Description	What it shows
Weighted connectivity length (WCL)	Average dispersal distance from origin to destination reef for all infectious elements released over a reef	Average distance at which a reef can send infectious matter
Out-degree	Number of out-going connections originating from a given reef multiplied by the total mass exchanged	Potential for a reef to spread the disease
Fraction exchanged	Fraction of infectious material produced on a given reef that settles on another reef	Success rate of potential disease spread
Self recruitment	Fraction of infectious material settling on a given reef that has been released on the same reef	Potential for disease to settle on a given reef

Table 1. Indicators used to analyze the modeled exchanges of infected material for each considered type of currents and for each simulated month

2.2   Epidemiological modeling

2.2.1   Model equations

The spread of the SCTLD throughout the FRT is simulated using a connectivity-based Kermack-McKendrick SIR model (Brauer, 2008). SIR models are among the most standard epidemiological models. They divide individuals into three compartments: susceptible (S), infectious (I) and removed (R). When affected by the disease, susceptible individuals become infectious and infect other susceptible individuals until they are removed, either by recovery or death. Such models usually rely on the hypothesis of an homogeneous, well-mixed population. To account for the spatial heterogeneity of the FRT, the basic SIR formulation is here modified by considering the proportions of susceptible (S_j), infectious (I_j) and removed (R_j) corals of each polygon reef j. In this epidemiological model, individual reefs interact through the exchange of infectious material as represented by the connectivity matrix. For each sub-reef j and at any time, the following relations hold: $0 \leq S_j, I_j, R_j \leq 1$ and $S_j + I_j + R_j = 1$. The evolution of these proportions through time is governed by the following equations:

$$\frac{dS_j}{dt} = -\beta \sum_i \frac{A_i}{A_j} I_i \tilde{C}_{ij} S_j - \beta'(I_j) S_j I_j$$

$$\frac{dI_j}{dt} = \beta \sum_i \frac{A_i}{A_j} I_i \tilde{C}_{ij} S_j + \beta'(I_j) S_j I_j - \sigma I_j \qquad (2)$$

$$\frac{dR_j}{dt} = \sigma I_j$$

where $\tilde{C}_{ij}$ is the entry of reef (i,j) of the normalized potential connectivity matrix [-], A_i is the area of reef polygon i [km^2], σ is the removal rate [day^{-1}], and β and $\beta'(I_j)$ are the inter- and intra-reef disease transmission rates [day^{-1}], respectively. In this model, infectious corals of reef i can infect corals of reef j if there is non-zero probability of infectious material exchange from reef i to reef j, given by $\tilde{C}_{ij}$. Moreover, to account for coral resistance to the disease, the intra-reef transmission function $\beta'(I_j)$ has the shape of a

181   smooth step function of the proportion of infectious corals I_j and writes:

$$\beta'(I_j) = \frac{\beta'_0}{2}(1 + \tanh[(I_j - I_0)/\tau]), \tag{3}$$

182   where I_0 is a threshold on the infection population above which intra-reef transmission becomes significant,
183   and τ is a measure of the interval over which the transition for low to high transmission occurs. As
184   long as the proportion of infectious corals on reef j is below I_0, the only infection mechanism taking
185   place is connectivity-driven transmission at rate β. Once the threshold is exceeded ($I_j \geq I_0$), intra-reef
186   transmission with rate β'_0 is activated. A larger value of threshold I_0 corresponds to a greater resistance to
187   disease for corals and therefore a slower spread of the disease within reef j. Coral birth and natural (*i.e.*
188   non SCTLD-related) death rates are not taken into account in this model, which amounts to assume that
189   they balance each other. For this study the same values were used for β and β'_0.

190   ## 2.2.2   Calibration

191   Transmission and removal parameters of σ and β'_0 are fitted to disease prevalence observations averaged
192   over all colonies from all monitored sites in the FRT in order to accurately simulate the temporal evolution
193   of S_j, I_j, R_j on each infected reef polygon. **[some details about parameter estimations from the meta-**
194   **analysis would be nice here]** To relate our model framework to the compiled data, Eqs. 2 are simplified
195   to a single-reef SIR model:

$$\frac{dS}{dt} = -\beta'_0 SI$$
$$\frac{dI}{dt} = \beta'_0 SI - \sigma I \tag{4}$$
$$\frac{dR}{dt} = \sigma I$$

196   Due to the low values of the entries in the normalized connectivity matrix $\tilde{C}_{ij}$, intra-reef transmission,
197   when activated, is the dominant infection mechanism of Eqs. 2. Consequently, Eqs. 4 give a reasonable
198   approximation of the evolution of the disease on sub-reefs for which $I_j > I_0$. Using this approximation,
199   the ratio β'_0/σ is imposed by matching the modeled proportion of susceptible corals remaining after the
200   disease has vanished (S_∞) with observations. A standard property of a SIR model solution is that

$$S_\infty - \frac{\sigma}{\beta'_0} \log(S_\infty/S_0) = 1 \tag{5}$$

201   where the initial proportion of susceptible corals (S_0) is taken equal to $1 - I_0$ (see for instance Murray
202   (2007)). In the framework of Eqs. 4, the ratio β'_0/σ gives the value of the basic reproduction number R_0,
203   defined as the average number of secondary cases produced by one infected individual introduced into a
204   population of susceptible individuals (Keeling and Rohani, 2007). This number is used in epidemiological
205   models to determine whether an emerging infectious disease can spread in a population ($R_0 > 1$) or not
206   ($R_0 < 1$). The obtained basic reproduction number is then used to express $\sigma\,in\,terms\,of\,\beta'_0$ and calibrate its
207   value in order to reproduce as well as possible the temporal evolution of the colonies-averaged susceptible
208   population shown in Fig. 5.

209   ## 2.2.3   Initialization

210   In order to solve Eqs. 2, initial conditions are needed, *i.e.* proportions of susceptible, infectious and
211   recovered corals at the beginning of the simulated period. This information is constructed based on different
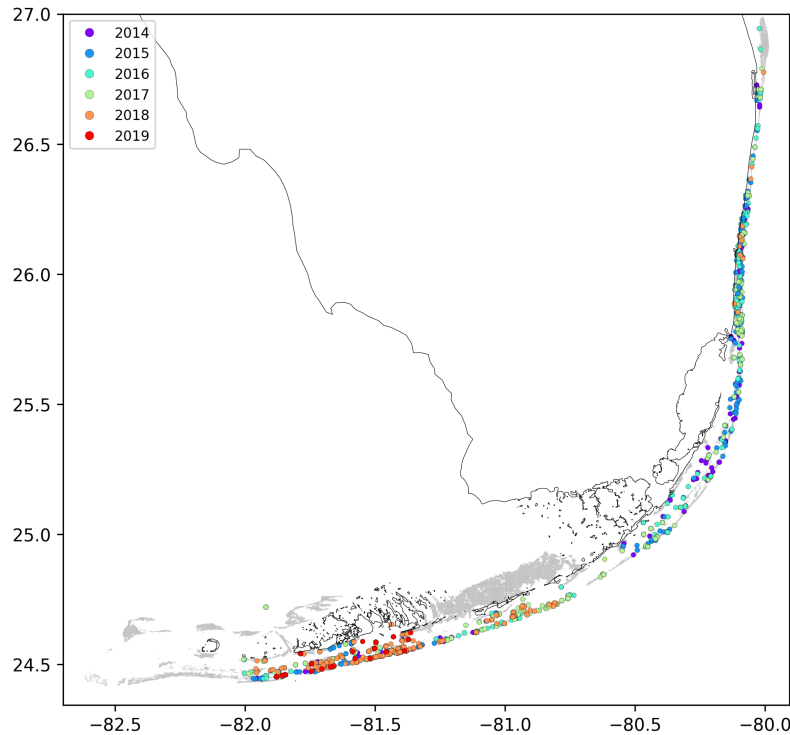
Figure 2. Locations of the disease observations between 2014 and 2019 recorded in the data sets used in this study

212 field-collected datasets: : (i) Coral Reef Evaluation and Monitoring Project (CREMP; 2014–2017), (ii)
213 CREMP Presence/Absence Data (CREMP P_A; 2016–2017), (iii) Southeast Florida Coral Reef Evaluation
214 and Monitoring Project (SECREMP; 2014– 2017), (iv) Florida Reef Resilience Program Disturbance
215 Response Monitoring (FRRP; 2014–2017), (v) Hurricane Irma Rapid Reef Assessment (IRMA; 2017,
216 Viehman et al. (2018)), (vi) the Southeast Florida Action Network citizen science program (SEAFAN;
217 2014–2017), and (vii) the Southern Coral Disease Margin field effort (2017; Neely (2018)). These datasets
218 give the locations and dates at which the SCTLD has been observed throughout the FRT. The locations
219 of these observations are shown in Fig. 2. Using this information, we first delineate an infected zone by
220 constructing the concave hull of the points where the disease was observed before May 2018. The reefs
221 infected prior to the beginning of our simulated period are then defined as the reefs located inside the
222 constructed zone. The time of observed infection is then spatially interpolated on each reef of the infected
223 zone by kriging with a Gaussian semivariogram using Python `pyKrige` module. Assuming an initial state
224 $(S, I, R) = (1 - I_0, I_0, 0)$ when the disease was observed, the proportions of susceptible, infectious and
225 removed corals on each reef of the infected zone on the 1st May 2018 is finally approximated using the
226 simplified equations 4. Reefs outside of the infected zone are initialized with a population of 100% of
227 susceptible corals.

228 2.2.4   Computation of front speed

229   Muller et al. (2020) estimated the speed of the spreading STCLD epidemics at around 92 m/day in the
230 southern section of the FRT. In order to assess our simulation results in regard to this value, we developed
231 a methodology to compute the displacement of the disease front during a given time interval within our
232 simulated period. First, the concave hull of the infected polygons at the beginning of the time interval H_0
233 is computed. Then the concave hull of the polygons infected during the time interval H_1 is computed while
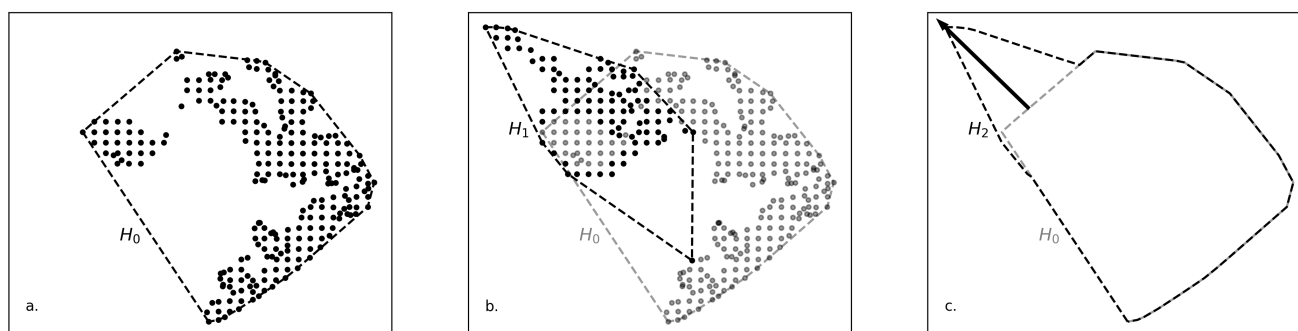
Figure 3. Method used to compute the disease front displacement during a simulated time interval.**a.** Concave hull of the infected polygons at the beginning of the simulated period H_0. **b.** Concave hull of the polygons infected during the simulated simulated H_1. **c.** Arrow showing the computed front displacement during simulated time interval between H_0 and H_2, the union of H_0 and H_1.

234 the concave hull H_2 is defined as the union of H_0 and H_1. This methodology is illustrated in Fig. 3. The
235 distance traveled by the disease front is then obtained by computing the maximum distance between a pair
236 of points of H_0 and H_2. The epidemics front speed is finally computed by dividing the resulting distance
237 by the number of days in the simulated time interval.

3 RESULTS

3.1 Exchanges of infected materials

239   Among the three modes of transport, bottom currents exhibit the lowest range as they generate the
240 networks with the smallest weighted connectivity length (Fig. 4). However, infectious matters transported
241 by bottom currents have the largest settlement success rate as these currents generate the graphs with the
242 largest fraction exchanged. Therefore, bottom currents tend to transport more infectious material on closer
243 reefs compared to the two other modes of transport.

244   Mean and surface currents, on the other hand show similar spreading ranges with mean WCL of 20.63 km
245 and 21.39 km respectively. However, the infectious matters that surface currents transport have the weakest
246 probability to successfully settle on reefs. Consequently, surface currents and bottom currents produce
247 networks with similar mean out-degree, although surface currents have the potential to transport infectious
248 matter on more reefs. Nonetheless, networks have larger median out-degree with bottom currents than
249 with surface currents, which suggests that surface currents have a lower spreading potential than bottom
250 currents. As a result of their large WCL and fraction exchanged, barotropic currents on the other hand
251 exhibit the largest mean out-degree, which suggest that they have a strong dispersal potential.

252   Self recruitment gives the proportion of infectious material settling on a reef that was produced on the
253 same reef. The greater its values, the more the reef is isolated from the rest of the network. Since infectious
254 material is less likely to settle on isolated reefs, self recruitment measures the probability for the disease to
255 settle on a given reef, whereas all three other indicators inform on the reef spreading potential. Fig. 4 shows
256 that the disease is more likely to settle on the reefs of networks generated by mean currents. This result is
257 consistent with the values of the other connectivity measures, as reefs tend to be more strongly connected
258 with mean currents. On the other hand, reefs are more isolated with bottom currents, as they produce the
259 graphs with lowest WCL and out-degree. Finally, surface currents generate larger self recruitment values
260 than mean currents as they exhibit the lowest fraction exchanged.
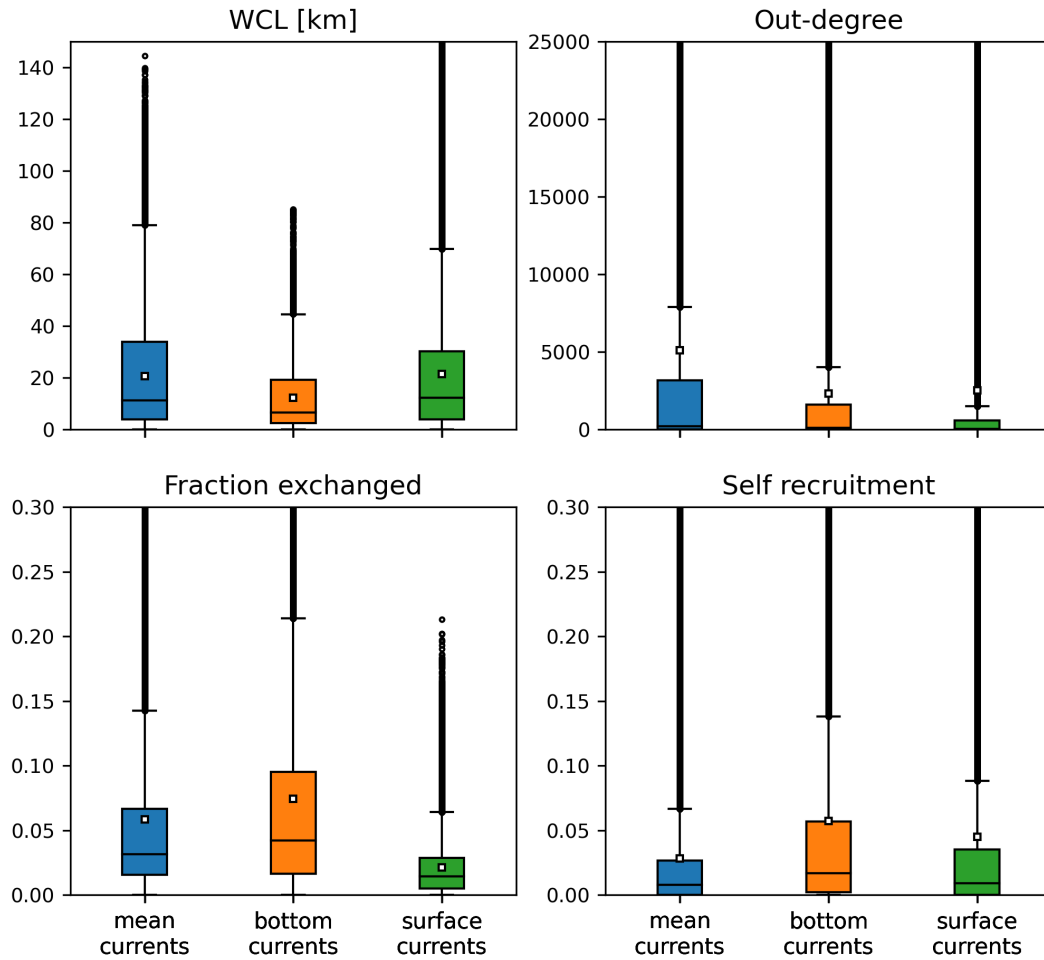
Figure 4. Distribution of the indicators derived from the monthly connectivity matrices computed for each type of current during our simulated period. Mean values are indicated by white squares

3.2 Epidemiological model results

Best fit to averaged disease prevalence observations is obtained with transmission rate $\beta_0^{-1\prime} = 6.45$ days and removal rate $\sigma^{-1} = 6.99$ days. Comparison of the evolution of the state described by Eqs 4 results with observations is shown in figure 5. Our model results accurately reproduce the observed fraction of susceptible individuals on colonies through time. However, the modeled fraction of removed individuals overestimates observations by about 5%. These discrepancies might be explained by the presence of "Unknown" values in our data sets as well as the simplifying assumptions of SIR models. Transmission and removal rates are found to have fairly close values with basic β_0'/σ being equal to 1.0345. This proximity in rate values is imposed by Eq. 5, as aggregated observations show a proportion of susceptible individuals of about 85% at the end of the outbreak. Since infection and removal occur at very close rates, the instantaneous proportion of infectious individuals on the reefs remains pretty low through the outbreak, with a maximum value of about 0.4%.

Using the above calibrated epidemiological parameters, epidemiological model simulations were performed from 1st May 2018 to 1st April 2019 for each type of currents and different values of the infection threshold I_0. A summary of the simulation results are shown in Fig. 6. Two metrics are used to assess the accuracy of the model. First, the modeled front speed is compared to the reference rate of 92
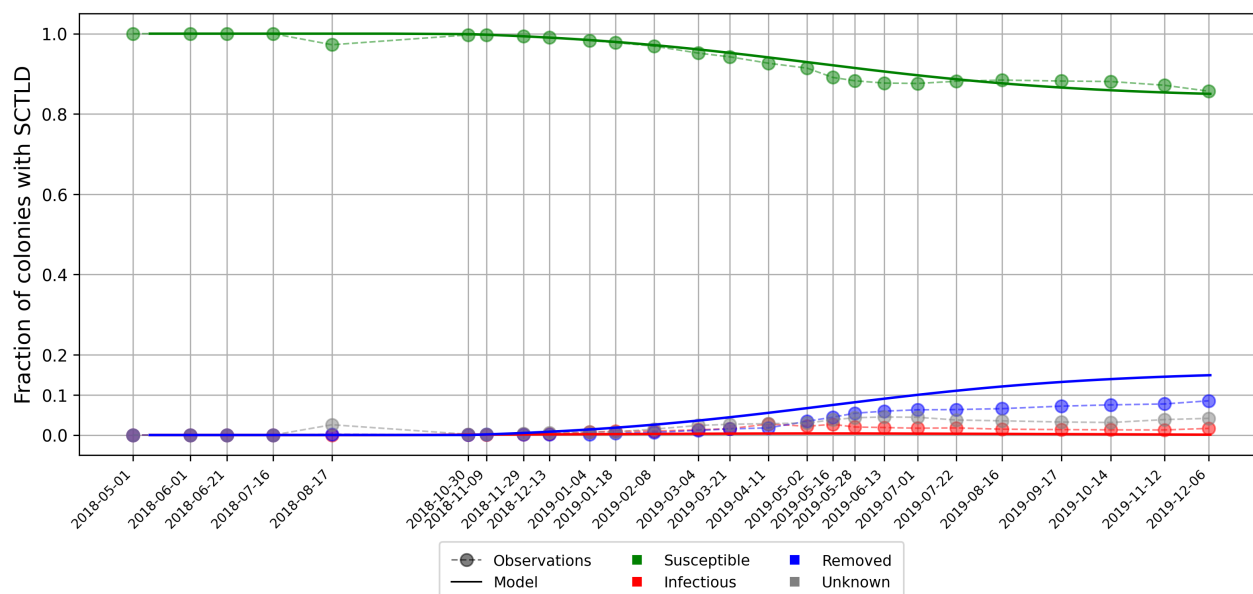
Figure 5. Disease prevalence averaged over all monitored sites over time as modeled by Eqs. 4 using calibrated transmission and removal parameters $\beta_0^{-1\prime} = 6.45$ days and $\sigma^{-1} = 6.99$ days.

277 m/day derived by Muller et al. (2020). Furthermore, we computed the mean of the distances between each
278 point where the SCTLD has been observed during our simulated period and the centroid of the closest reef
279 polygon predicted to be infected by our model during the same period. Bottom currents produce the slowest
280 modeled disease propagation with a maximum front speed of ~ 20 m/day, while simulations performed
281 with surface currents spread the disease at a maximum speed of of about 60 m/day. However, surface
282 currents tend to propagate the disease to the north, rather than westward, along the Florida Keys. This
283 explains why bottom currents predict infection closer to observations despite exhibiting slower front speed.
284 Finally, Mean barotropic currents outperform other types of current regarding both criteria with a front
285 speed of 107 m/day and a mean geographical accuracy of ~ 1.2 km. This suggest that the causative agent
286 of the disease might be transported within neutrally buoyant material driven from reef to reef inside the
287 water column by mean currents.

288 Moreover, Fig. 6 shows a strong dependence of model results to infection threshold I_0, that gives
289 the proportion of infectious individual that colonies can withstand before exponential disease growth is
290 triggered on reef. Front speeds of both mean and bottom currents reach a plateau for values of infection
291 threshold between $I_0 = 0.05\%$ and $I_0 = 0.1\%$, while the minimal prediction error is attained around
292 $I_0 \approx 0.078\%$ with mean currents. For $I_0 > 0.1\%$, intra-reef infection is strongly impeded and populations
293 of infectious individuals on infected reefs are not able to become sufficiently large to infect other colonies
294 on reefs they are connected to. For values of I_0 lower than 0.05% on the other hand, intra-reef infection
295 dominates and coral population on infected reefs is removed too fast to efficiently spread the disease
296 through the network. Since disease propagation throughout the FRT only occurs for fairly small values of
297 I_0 in our model, corals are expected to have low resistance to the causative agent of the SCTLD.

298 The results shown in Fig. 6 were obtained by removing the large reef located North to Vaca key, denoted
299 Vaca reef in Frys et al. (2020), from our reef polygons. Preliminary simulations showed that this reef
300 has close to no impact on the modeled spread of the disease to the rest of the FRT, as it sends very little
301 infectious material to southerly and easterly neighboring reefs. Moreover, Vaca reef has a low coral coverage
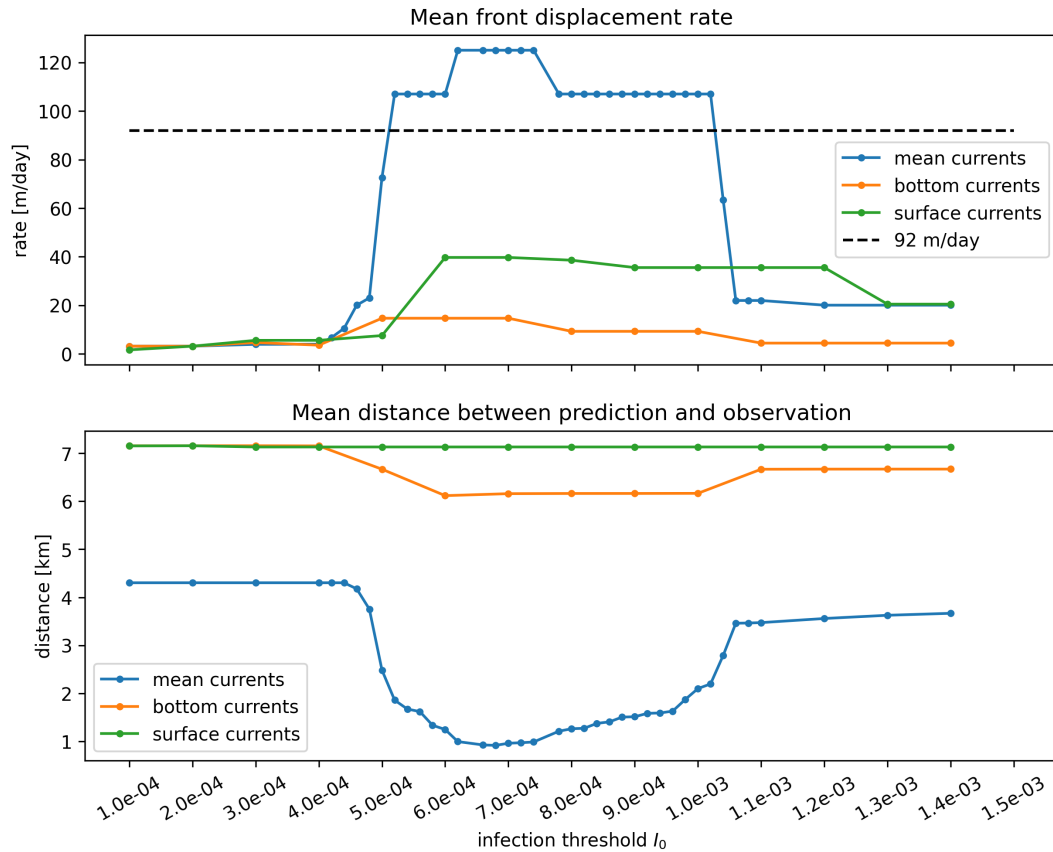
Figure 6. Summary of epidemiological model simulations with calibrated transmission parameters. **Top:** Modeled disease front speed for each type of current with respect to intra-reef infection threshold I_0. **Bottom:** Mean distance between predicted infected reefs and observed disease points. These results show that mean barotropic currents outperform other modes of transport at reproducing the observed spread of the disease. The appearance of a plateau suggests that model predictions are very sensitive to the value of the infection threshold I_0.

302 $(0 - 10\%)$, which strongly impedes disease spread on the reef. However, as coral coverage is not taken into
303 account in our epidemiological model, propagation of the disease on the reef was overestimated. This led
304 to unrealistically strong modeled front speed variations due to the large size of the reef. Consequently, and
305 in the absence of SCTLD observations on Vaca reef, it has been removed from our reef polygons in order
306 to avoid overestimating the front speed.

4 DISCUSSION AND CONCLUSIONS

307 We have developed an epidemio-hydrodynamic model to simulate the spread of the SCTLD through
308 the entire FRT. Calibrating our model with colonies-averaged prevalence observations, we estimate the
309 species-averaged reproduction number R_0 to be barely larger than one. Our model simulations suggest
310 that only the barotropic currents are able to reproduce the observed spread of the disease. Bottom current
311 do not spread infectious material far enough while surface currents do not allow infectious material to
312 spend enough time over the reefs to strongly infect them. The causative agent of the SCTLD is therefore
313 expected to be transported within neutrally buoyant particles inside the water column. With this mode of
314 transport, the propagation of the disease from reef to reef only occurs for a well-defined range of values of
315 the infection threshold I_0. This threshold is defined as the proportion of colonies that have to be infected

316 to trigger a rapid spread of the disease over the entire reef. Our result suggest that this occurs as soon as
317 $0.05 - 0.1\%$ of colonies are infected. On average, corals are thus expected to a have low resistance to the
318 SCTLD.

319   After calibration, we estimated the species-averaged basic reproduction number β'_0/σ to be equal to
320 1.0835. This value being close to 1, modeled infectious individuals are removed from the system almost
321 as fast as susceptible individuals get infected. This causes the proportion of infectious corals on the reefs
322 to remain pretty low (*i.e.* $\leq 0.4\%$) through time. This suggests that only a small fraction of the colony
323 causes the disease to spread on the reef during the outbreak. **[add some comments on tank experiments**
324 **+ comparison with model results]**. In this study, the same values were used for inter- and intra-reef rates
325 β and β'_0. This implies that the infectiousness of the causative agent is not reduced during its journey
326 from reef to reef. However, to assess the impact of this assumption, epidemiological model simulations
327 were performed with $\beta = \beta'_0/2$. The resulting disease front speeds did not exceed 20 m/day. This strong
328 decrease can be explained by the interplay between inter- and intra- reef infection. Reducing inter-reef
329 transmission rates decreases the proportion of infectious corals on reefs attained by infectious materials,
330 which in turn reduces the amount of infectious matter sent to the rest of the network. This suggests that, to
331 reproduce the observed spread, inter- and intra-reef transmission rates must have similar magnitude, *i.e.*
332 that the causative agent is almost not degraded while traveling from reef to reef. **Is this consistent with**
333 **Rhodobacterales and Rhizobiales ?**

334   The fact that mean barotropic currents outperform the other modes of transport can be explained by
335 considering the trajectories of the particles used to model the transport of the vector of the disease causative
336 agent. Due to the impact of winds on positively buoyant materials, particles driven by surface currents
337 are likely to be blown away from the reefs. Moreover, even when winds are pushing particles along the
338 reef line, these particles spend less time over the same region than particles driven by mean and bottom
339 currents. Smaller amounts of particle mass will therefore settle on reef polygons, leading to lower entries
340 of the potential connectivity matrix, *i.e.* lower exchange of infectious material between reefs. Hence,
341 despite being able to transport the disease over greater distances, surface currents are less likely to drive
342 the propagation of the disease. Particles driven by bottom currents, on the other hand, remain longer over
343 the same region, producing larger entries of the potential connectivity matrix. Due to these large exchange
344 probabilities between reefs, bottom currents are better at propagating the disease (Fig. 6). Nevertheless,
345 bottom currents being relatively slower, exchanges of infected materials occur on a limited geographical
346 range. Mean barotropic currents, that carry particles on greater distances while allowing for sufficiently
347 large amounts of infected mass to settle on reef polygons, are thus best suited to propagate the disease (Fig.
348 6).

349   Since mean currents are the only mode of transport that successfully reproduces the observed propagation
350 speed of the disease in our model, the disease causative agent is expected to be transported within neutrally
351 buoyant material inside the water column. This assumption seems reasonable as water-borne transmission
352 is implicated as an important spreading mechanism for multiple coral diseases *(OK but could surface*
353 *or bottom currents as well...)*, including white band disease, white plague disease, white pox disease,
354 white syndrome disease, *Porites* ulcerative white spots diseases, skeletal eroding band disease (Shore and
355 Caldwell, 2019). **[examples of neutrally buoyant vectors ? mucus ?]**. The causative agent might also be
356 transported within fine sediments such as silt, as suggested by Rosales et al. (2020). Such sediments are
357 easily eroded in shallow areas around coral reefs and would therefore be mostly transported inside the water
358 column by mean barotropic currents. This hypothesis might be tested by adapting the deposition rate γ used
359 in our experiments to be consistent with the sedimentation rate of silt. However, such modification of γ

360 would alter the entries of our potential connectivity matrices. Nonetheless, the sensitivity of the connectivity
361 matrices to the value of γ has been briefly assessed by generating new matrices using particles with a
362 half-life of 15 days (γ increased by a factor two). Although these matrices exhibited stronger short-range
363 connectivity, the impact on connectivity indicator values remained limited ($< 10\%$). This suggests that the
364 main results of this study would remain valid for fine sediments.

365 Coral resistance to the SCTLD in represented by parameter I_0, defined as the maximum proportion
366 of the colony that can get infected without causing the disease to spread to the rest of the colony. The
367 plateau shown in Fig. 6 highlights the impact of this parameter on the modeled propagation of the disease.
368 On the one hand, when corals are strongly susceptible to the disease, infectious individuals are removed
369 from the system too fast to become sustainable sources of infectious materials in the network. On the
370 other hand, if corals are weakly susceptible to the disease, very few corals get infected and the disease
371 barely propagates. Our simulations suggest that this value must be fairly low (around 0.01%) in order to
372 successfully spread the disease throughout the FRT. **This seems to imply that susceptible coral species**
373 **have very weak defense mechanisms against the causative agent of the disease. (?)**.
374

375 As with any modeling study, it is important to understand the assumptions on which the model is based.
376 Here, we have used a 2D barotropic ocean model coupled with the 3D model HYCOM (Chassignet et al.,
377 2007) in order to indirectly represent baroclinic phenomena. Such model is well suited to simulate the fate
378 of neutrally-buoyant matters in shallow regions. However, as depth-averaged currents do not accurately
379 approximate the motion of particles in the bottom and surface layers, SLIM velocities have therefore been
380 modified to simulate the exchanges of negatively and positively buoyant matters. Surface current response
381 to wind parametrization is based on the results of Ardhuin et al. (2009), consistent with observations. In
382 this study, measured surface currents are shown to be in the order of $1.0\% - 1.8\%$ of the wind speed, in a
383 direction $10° - 40°$ to the right of the wind. **[discuss bottom currents parametrization]**. Although such
384 estimation of surface and bottom currents is disputable, using a 2D model allows for reef-scale resolution
385 throughout the whole FRT. Such high-resolution allows to capture recirculation eddies around islands and
386 reefs, that significantly impact the weighted connectivity length as well as the local retention on the reefs.

387 The appearance of an interval of optimal values of threshold I_0 for the propagation of the disease in our
388 results highlights the impact of coral resistance on the spread of SCTLD through the FRT. Therefore, a
389 further step in our modeling approach would be further dividing coral populations of our polygons into
390 highly susceptible (*e.g. Dichocoenia stokesii*, *Meandrina meandrites*), intermediately susceptible (*e.g.*
391 *Orbicella faveolata*, *Montastrea cavernosa*), and weakly susceptible (*e.g. Acropora Palmata*, *Acropora*
392 *cervicornis*) sub-populations. The proportions susceptible, infectious and removed individuals within these
393 sub-populations would then be modeled with specific transmission (β, β_0') and removal (σ) rates as well as
394 specific infection thresholds I_0. Such approach would however require a fine knowledge of the distribution
395 of the different coral species throughout the FRT. This knowledge about coral coverage could also be used
396 to avoid overestimation of the front propagation, as in the case of Vaca reef.

397 Despite the limitations of its current formulation, we believe that our model brings unprecedented
398 perspectives on the propagation mechanism of the SCTLD through the FRT. Using a reef-scale spatial
399 resolution, we determined the most probable mode of transport for the vector of the disease agent and
400 deduced its species-averaged reproduction number based on prevalence observations. Besides, our model
401 formulation provides a framework to quantity coral resistance to the disease. As our model results are
402 continuous through time, they can exhibit the variability of the propagation of the SCTLD through time
403 and therefore bring additional insight to observation data. This study therefore provides much-needed

404 complementary insight on the identification of the causative agent of the Stony Coral Tissue Loss disease
405 and the management of the crisis it generates. *Say that our approach could be applied to other areas aw*
406 *well where there is still time to do active management of the disease.*

CONFLICT OF INTEREST STATEMENT

407 The authors declare that the research was conducted in the absence of any commercial or financial
408 relationships that could be construed as a potential conflict of interest.

AUTHOR CONTRIBUTIONS

FUNDING

ACKNOWLEDGMENTS

REFERENCES

413 Aeby, G., Ushijima, B., Campbell, J. E., Jones, S., Williams, G., Meyer, J. L., et al. (2019). Pathogenesis of
414   a tissue loss disease affecting multiple species of corals along the florida reef tract. *Frontiers in Marine*
415   *Science* 6, 678
416 Alvarez-Filip, L., Estrada-Saldívar, N., Pérez-Cervantes, E., Molina-Hernández, A., and González-Barrios,
417   F. J. (2019). A rapid spread of the stony coral tissue loss disease outbreak in the Mexican Caribbean.
418   *PeerJ* 7, e8069
419 Ardhuin, F., Marié, L., Rascle, N., Forget, P., and Roland, A. (2009). Observation and estimation of
420   Lagrangian, Stokes, and Eulerian currents induced by wind and waves at the sea surface. *Journal of*
421   *Physical Oceanography* 39, 2820–2838
422 Aronson, R. B. and Precht, W. F. (2001). White-band disease and the changing face of Caribbean coral
423   reefs. In *The ecology and etiology of newly emerging marine diseases* (Springer). 25–38
424 Aronson, R. B. and Precht, W. F. (2006). Conservation, precaution, and Caribbean reefs. *Coral reefs* 25,
425   441–450
426 Bidegain, G., Powell, E., Klinck, J., Ben-Horin, T., and Hofmann, E. (2016a). Microparasitic disease
427   dynamics in benthic suspension feeders: infective dose, non-focal hosts, and particle diffusion. *Ecological*
428   *modelling* 328, 44–61
429 Bidegain, G., Powell, E. N., Klinck, J. M., Ben-Horin, T., and Hofmann, E. E. (2016b). Marine infectious
430   disease dynamics and outbreak thresholds: contact transmission, pandemic infection, and the potential
431   role of filter feeders. *Ecosphere* 7, e01286
432 Blondeau, J., Brandt, M., Donovan, C., Eakin, M., Edwards, K., Edwards, K., et al. (2020). Coral reef
433   condition: A status report for the US Virgin Islands
434 Brandt, M. E. and McManus, J. W. (2009). Dynamics and impact of the coral disease white plague: insights
435   from a simulation model. *Diseases of aquatic organisms* 87, 117–133

Brauer, F. (2008). Compartmental models in epidemiology. In *Mathematical epidemiology* (Springer). 19–79

Burgess, S. C., Kingsford, M. J., and Black, K. P. (2007). Influence of tidal eddies and wind on the distribution of presettlement fishes around One Tree Island, Great Barrier Reef. *Marine Ecology Progress Series* 341, 233–242

Chassignet, E. P., Hurlburt, H. E., Smedstad, O. M., Halliwell, G. R., Hogan, P. J., Wallcraft, A. J., et al. (2007). The HYCOM (hybrid coordinate ocean model) data assimilative system. *Journal of Marine Systems* 65, 60–83

Dustan, P. and Halas, J. C. (1987). Changes in the reef-coral community of Carysfort Reef, Key Largo, Florida: 1974 to 1982. *Coral Reefs* 6, 91–106

Figueiredo, J., Baird, A. H., and Connolly, S. R. (2013). Synthesizing larval competence dynamics and reef-scale retention reveals a high potential for self-recruitment in corals. *Ecology* 94, 650–659

Frys, F., Saint-Amand, A., Le Hénaff, M., Figueiredo, J., Kuba, A., Walker, B., et al. (2020). Fine-scale coral connectivity pathways in the Florida Reef Tract: Implications for conservation and restoration. *Frontiers in Marine Science* in press. doi:10.3389/fmars.2020.00312

FWC, F. (2017). Unified reef map v2. 0

Gardner, T. A., Côté, I. M., Gill, J. A., Grant, A., and Watkinson, A. R. (2003). Long-term region-wide declines in Caribbean corals. *science* 301, 958–960

Geuzaine, C. and Remacle, J.-F. (2009). Gmsh: A 3-d finite element mesh generator with built-in pre-and post-processing facilities. *International journal for numerical methods in engineering* 79, 1309–1331

Harvell, D., Jordán-Dahlgren, E., Merkel, S., Rosenberg, E., Raymundo, L., Smith, G., et al. (2007). Coral disease, environmental drivers, and the balance between coral and microbial associates. *Oceanography* 20, 172–195

Keeling, M. and Rohani, P. (2007). Stochastic dynamics. *Modeling Infectious Diseases in Humans and Animals* , 190–230

Kourafalou, V. H. and Kang, H. (2012). Florida current meandering and evolution of cyclonic eddies along the Florida Keys Reef Tract: Are they interconnected? *Journal of Geophysical Research: Oceans* 117

Kuffner, I. B., Lidz, B. H., Hudson, J. H., and Anderson, J. S. (2015). A century of ocean warming on florida keys coral reefs: historic in situ observations. *Estuaries and Coasts* 38, 1085–1096

Kuta, K. and Richardson, L. (1996). Abundance and distribution of black band disease on coral reefs in the northern Florida Keys. *Coral reefs* 15, 219–223

Lambrechts, J., Hanert, E., Deleersnijder, E., Bernard, P.-E., Legat, V., Remacle, J.-F., et al. (2008). A multi-scale model of the hydrodynamics of the whole Great Barrier Reef. *Estuarine, Coastal and Shelf Science* 79, 143–151

Manzello, D. P. (2015). Rapid recent warming of coral reefs in the Florida Keys. *Scientific reports* 5, 16762

Miller, J., Muller, E., Rogers, C., Waara, R., Atkinson, A., Whelan, K., et al. (2009). Coral disease following massive bleaching in 2005 causes 60% decline in coral cover on reefs in the US Virgin Islands. *Coral Reefs* 28, 925

Muller, E. M., Sartor, C., Alcaraz, N. I., and van Woesik, R. (2020). Spatial epidemiology of the Stony-Coral-Tissue-Loss Disease in Florida. *Frontiers in Marine Science* 7, 163

Murray, J. D. (2007). *Mathematical biology: I. An introduction*, vol. 17 (Springer Science & Business Media)

Neely, K. (2018). Surveying the Florida Keys southern coral disease boundary. *Florida DEP. Miami, FL* , 1–15

481 NOAA (2018). *Stony Coral Tissue Loss Disease Case Definition* . Available online at:
482 `https://nmsfloridakeys.blob.core.windows.net/floridakeys-prod/media/`
483 `docs/20181002-stony-coral-tissue-loss-disease-case-definition.pdf`
484 (accessed June 4, 2020)

485 Porter, J. W. and Meier, O. W. (1992). Quantification of loss and change in floridian reef coral populations.
486 *American Zoologist* 32, 625–640

487 Precht, W. F., Gintert, B. E., Robbart, M. L., Fura, R., and Van Woesik, R. (2016). Unprecedented
488 disease-related coral mortality in southeastern florida. *Scientific Reports* 6, 1–11

489 Richardson, L. L., Goldberg, W. M., Kuta, K. G., Aronson, R. B., Smith, G. W., Ritchie, K. B., et al. (1998).
490 Florida's mystery coral-killer identified. *Nature* 392, 557–558

491 Rosales, S. M., Clark, A. S., Huebner, L. K., Ruzicka, R. R., and Muller, E. (2020). Rhodobacterales and
492 Rhizobiales are associated with stony coral tissue loss disease and its suspected sources of transmission.
493 *Frontiers in Microbiology* 11, 681

494 Ruzicka, R., Colella, M., Porter, J., Morrison, J., Kidney, J., Brinkhuis, V., et al. (2013). Temporal changes
495 in benthic assemblages on florida keys reefs 11 years after the 1997/1998 el niño. *Marine Ecology*
496 *Progress Series* 489, 125–141

497 Shore, A. and Caldwell, J. M. (2019). Modes of coral disease transmission: How do diseases spread
498 between individuals and among populations? *Marine biology* 166, 45

499 Sokolow, S. (2009). Effects of a changing climate on the dynamics of coral infectious disease: a review of
500 the evidence. *Diseases of Aquatic Organisms* 87, 5–18

501 Sponaugle, S., Paris, C., Walter, K., Kourafalou, V., and Alessandro, E. (2012). Observed and modeled
502 larval settlement of a reef fish to the Florida Keys. *Marine Ecology Progress Series* 453, 201–212

503 Sutherland, K. P., Porter, J. W., and Torres, C. (2004). Disease and immunity in Caribbean and Indo-Pacific
504 zooxanthellate corals. *Marine Ecology Progress Series* 266, 273–302

505 Team, A. B. R. (2005). Atlantic Acropora status review document. *Report to National Marine Fisheries*
506 *Service* , 152

507 Thomas, C. J., Bridge, T. C., Figueiredo, J., Deleersnijder, E., and Hanert, E. (2015). Connectivity between
508 submerged and near-sea-surface coral reefs: Can submerged reef populations act as refuges? *Diversity*
509 *and Distributions* 21, 1254–1266

510 Thomas, C. J., Lambrechts, J., Wolanski, E., Traag, V. A., Blondel, V. D., Deleersnijder, E., et al. (2014).
511 Numerical modelling and graph theory tools to study ecological connectivity in the Great Barrier Reef.
512 *Ecological Modelling* 272, 160–174

513 Vaz, A. C., Paris, C. B., Olascoaga, M. J., Kourafalou, V. H., Kang, H., and Reed, J. K. (2016). The perfect
514 storm: match-mismatch of bio-physical events drives larval reef fish connectivity between Pulley Ridge
515 mesophotic reef and the Florida Keys. *Continental Shelf Research* 125, 136–146

516 Viehman, S., Gittings, S., Groves, S., Moore, J., Moore, T., and Stein, J. (2018). NCCOS Assessment: Coral
517 Disturbance Response Monitoring (DRM) Along the Florida Reef Tract Following Hurricane Irma From
518 2017-10-09 to 2017- 10-18 (NCEI Accession 0179071). *NOAA National Centers for Environmental*
519 *Information* . Silver Spring, MD: National Centers for Coastal Ocean Science. Available online at:
520 `https://doi.org/10.25921/sscd-6h41`

521 Wolanski, E. (1994). *Physical oceanographic processes of the Great Barrier Reef* (CRC Press)

TABLES AND FIGURES